HHS Public Access

Author manuscript

Exp Cell Res. Author manuscript; available in PMC 2022 June 01.

Published in final edited form as:

Exp Cell Res. 2021 June 01; 403(1): 112581. doi:10.1016/j.yexcr.2021.112581.

NF-κB activation in retinal microglia is involved in the inflammatory and neovascularization signaling in laser-induced choroidal neovascularization in mice

Fumihito Hikage[1], **Anton Lennikov**[2,3,*], **Anthony Mukwaya**[4], **Mieszko Lachota**[5], **Yosuke Ida**[1], **Tor Paaske Utheim**[6,7], **Dong Feng Chen**[3], **Hu Huang**[2], **Hiroshi Ohguro**[1]

[1]Department of Ophthalmology, School of Medicine, Sapporo Medical University, Sapporo, Japan

[2]University of Missouri-Columbia, Missouri, United States of America

[3]Department of Ophthalmology, Schepens Eye Research Institute of Massachusetts Eye and Ear, Harvard Medical School, Boston, Massachusetts, United States

[4]Department of Ophthalmology, Institute for Clinical, and Experimental Medicine, Faculty of Health Sciences, Linköping University, Linköping, Sweden.

[5]Department of Clinical Immunology, Doctoral School, Medical University of Warsaw, Warsaw, Poland

[6]Department of Ophthalmology, Oslo University Hospital, University of Oslo, Oslo, Norway

[7]Department of Medical Biochemistry, Oslo University Hospital, University of Oslo, Oslo, Norway

Abstract

[*]Corresponding author: Anton Lennikov, Schepens Eye Research Institute, 20 Staniford St, Boston, MA 02114, anton_lennikov@meei.harvard.edu.

Authors' contributions

The study was conceived and designed by AL, FH, and OH. AL, AM, ML conducted the in vitro experiments. FH, YI, AL, HH, and conducted the mouse *in vivo* studies. FH, AL, AM, YI. performed the *ex vivo* experiments and evaluations. The manuscript was written by FH, YI, AL, AM, ML, TPU, DFC and OH, and was critically revised by HH, TPU, DFC, and OH. All authors reviewed and accepted the final version of the manuscript.

Fumihito Hikage: Investigation, Methodology, Writing- Original draft preparation. **Anton Lennikov**: Conceptualization, Investigation, Investigation, Methodology, Writing- Original draft preparation, Funding acquisition, Visualization, Writing- Reviewing and Editing, Supervision. **Anthony Mukwaya**: Investigation, Writing- Original draft preparation. **Mieszko Lachota:** Investigation, Writing- Original draft preparation. **Yosuke Ida:** Investigation. **Tor Paaske Utheim:** Conceptualization, Writing- Reviewing and Editing. **Dong Feng Chen:** Conceptualization, Writing- Reviewing and Editing. **Hu Huang:** Conceptualization, Investigation, Writing- Reviewing and Editing, Funding acquisition. **Hiroshi Ohguro:** Conceptualization, Methodology, Writing- Original draft preparation, Writing- Reviewing and Editing, Supervision.

Ethics approval

In vivo experiments were approved by the Institutional Animal Care and Use Committee of the University of Missouri School of Medicine (protocol number: 9520) and by the Sapporo Medical University School of Medicine Ethics Committee. All experiments were in accordance with the guidelines of the Association for Research in Vision and Ophthalmology Statement for the use of animals in ophthalmic and vision research.

Financial interest statement

The authors have no financial interests to disclose in relation to this paper.

Conflict of interest statement

The authors have no conflicts of interest to disclose in relation to this paper.

Purpose: To evaluate Nuclear Factor NF-κB (NF-κB) signaling on microglia activation, migration, and angiogenesis in laser-induced choroidal neovascularization (CNV).

Methods: Nine-week-old C57BL/6 male mice were randomly assigned to IMD-0354 treated or untreated groups (5 mice, 10 eyes per group). CNV was induced with a 532-nm laser. Laser spots (power 250 mW, spot size 100 μm, time of exposure 50 ms) were created in each eye using a slit-lamp delivery system. Selective inhibitor of nuclear factor kappa-B kinase subunit beta (IKK2) inhibitor IMD-0354 (10 μg) was delivered subconjunctivally; vehicle-treated mice were the control. The treatment effect on CNV development was assessed at five days post-CNV induction *in vivo* in C57BL/6 and Cx3cr1$^{gfp/wt}$ mice by fluorescent angiography, fundus imaging, and *ex vivo* by retinal flatmounts immunostaining and western blot analysis of RPE/Choroidal/Scleral complexes (RCSC) lysates. *In vitro* evaluations of IMD-0354 effects were performed in the BV-2 microglial cell line using lipopolysaccharide (LPS) stimulation.

Results: IMD-0354 caused a significant reduction in the fluorescein leakage and size of the laser spot, as well as a reduction in microglial cell migration and suppression of phospho-IκBα, Vascular endothelial growth factor (VEGF-A), and Prostaglandin-endoperoxide synthase 2 (COX-2). *In vivo* and *ex vivo* observations demonstrated reduced lesion size in mice, CD68, and Allograft inflammatory factor 1 (IBA-1) positive microglia cells migration to the laser injury site in IMD-0354 treated eyes. The data further corroborate with GFP-positive cells infiltration of the CNV site in Cx3cr1$^{wt/gfp}$ mice. *In vitro* IMD-0354 (10–25 ng/ml) treatment reduced NF-κB activation, expression of COX-2, caused decreased Actin-F presence and organization, resulting in reduced BV-2 cells migration capacity.

Conclusion: The present data indicate that NF-κB activation in microglia and it's migration capacity is involved in the development of laser CNV in mice. Its suppression by IMD-0354 might be a promising therapeutic strategy for wet AMD.

Graphical abstract

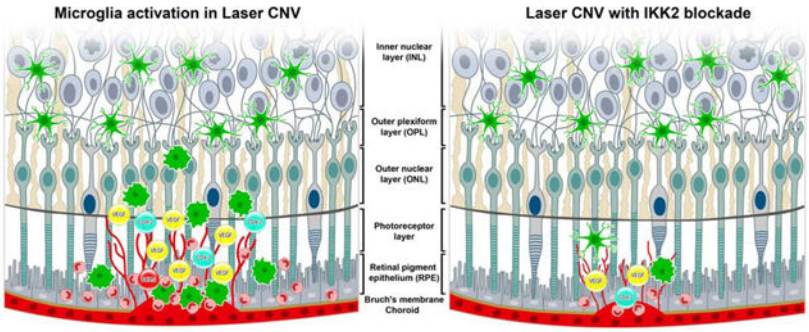

Keywords

laser CNV; retina; IKK-β; IKK2; NF-κB; microglia; IMD-0354

Introduction

Age-Related Macular Degeneration (AMD) is one of the leading causes of visual loss among people over 50 years of age [1]. Choroidal neovascularization (CNV) secondary to

AMD accounts for most cases of AMD-related severe vision loss. It is well documented that vascular endothelial growth factor (VEGF) is a critical molecule in CNV formation, with treatments such as humanized anti-VEGF antibody fragments [2]. However, in recent years there has been widespread concern that long-term inhibition of all VEGF isoforms may cause ocular complications [3, 4] and unexpected systemic consequences due to the inhibition of the physiological roles of VEGF such as vessel maintenance [5, 6]. Routine intraocular injections of anti-VEGF result in complications such as an increase in intraocular pressure [7] and ocular infection [8], along with anti-VEGF therapy resistance [9]. Such drawbacks led to the search for different approaches to CNV treatment.

Inflammation in the retina is associated with differential Nuclear Factor NF-κB (NFκB) activation based on the cell type involved [10]. While neuronal NF-κB activation is linked to increased cell survival, in microglia, it leads to proinflammatory cell activation and neuronal damage through the production of neurotoxic and proinflammatory cytokines [11, 12]. Recently we also demonstrated the relations between calcium ion influx through L-voltage-gated calcium channels (L-VGCC) and microglia proinflammatory state strongly associated with NF-κB activation [13].

IMD-0354 is a non-ATP binding competitive selective nuclear factor κ-B kinase subunit β (IKK2 also known as IKK-β) inhibitor, particularly when it is induced by proinflammatory cytokines, such as Tumor necrosis factor-α (TNF-α) and Interleukin-1β (IL-1β) [14–16]. Recent reports have shown that IMD-0354 is effective in acute and subacute inflammatory diseases, such as myocardial ischemia/reperfusion injury [15], insulin resistance [17], allergic inflammation in an acute mouse model of asthma [16]. We demonstrated that IMD-0354 effectively ameliorates endotoxin-induced uveitis by inhibiting inflammatory cells' infiltration of the ciliary body and reduced TNFα and CCL2 in aqueous humor [18]. We further reported the ameliorative effect of systemic IMD-0354 on vascular permeability in streptozotocin-induced diabetic retinopathy in mice through inhibition of VEGF-A and reduced retinal cell apoptosis. Previously we found NF-κB activation-driven expression of proinflammatory signalings such as chemokine (C–C motif) ligand 2 (CCL2; MCP-1) and C-X-C motif chemokine 5 (CXCL5; ENA78) in human umbilical vein endothelial cells (HUVEC) *in vitro* and confirmed these findings in suture induced corneal neovascularization model in rats [19].

Laser-induced CNV is a well-established model of inflammatory choroidal neovascularization in different animal species. It partially mimics the biochemical and immunological process of wet AMD in humans with neovascularization response develop at 14–15 post-laser injury [20]. Cx3cr1$^{gfp/gfp}$ mice are generated by the insertion of green fluorescent protein (GFP) to the Cx3cr1 locus that results in Cx3cr1 knock-out and expression of GFP in monocytes, dendritic cells, natural killer (NK) cells, and brain microglia under the control of the endogenous Cx3cr1 promoter [21]. Previously, we reported the correlation of CNV severity with GFP-positive cells infiltration into the laser spots in Cx3cr1$^{gfp/+}$ mice in the laser CNV model [22].

In the present study, we evaluated the effect of NF-κB inhibition on activation and migration of the microglia cells *in vivo* using laser CNV using an early time point of 5 days at the peak

of the inflammatory response, preceding the neovascularization process as well as *in vitro* using a BV-2 mouse microglia cell line.

Results

Inhibition of IKK2 reduces the size of CNV lesions and vascular leakage

Five days after laser exposure, leakage of fluorescein at the laser spot was observed in the CNV control mice (Fig. 1A); however, mice that received a subconjunctival injection of 10 μg IMD-0354 demonstrated reduced leakage (Fig. 1B). *Ex vivo* analysis of the laser spot size was consistent with the reduced fluorescein leakage areas (Fig 1C, D) in IMD-0354 treated eyes. Quantification of the spot area surface demonstrated a significant decrease in the laser CNV spot size ($p < 0.001$, Fig. 1E).

IKK2 inhibition results in reduced NF-κB activation, Prostaglandin-endoperoxide synthase 2 (COX-2), and VEGF-A expression

Immunohistochemical analysis of the retinal pigment epithelial–choroidal–scleral complexes (RCSC) indicated Allograft inflammatory factor 1 (IBA-1) positive microglia presence within with the laser spot (Fig 2A) with NF-κB activation within the microglia cells (Fig. 2A), consistent with the *in vivo* observations shown in Fig. 1A above. IMD-0354 treatment resulted in markedly reduced IBA-1 positive microglia cells presence and reduced nuclear localization of NF-κB. (Fig. 2B). Quantitative analysis NF-κB positive nuclei (Fig. 2C) demonstrated a significant difference ($p < 0.001$) between the control and treated groups. The representative images NF-κB/DAPI double-stained RCSC are present in Fig. S1. Western blot analysis of the RCSC lysates indicated an increase of phosphorylated IκBα (p-IκBα) and VEGF-A in laser CNV samples compared to the naïve control sample, IMD-0354 treatment, reduced the presence of both p-IκBα and VEGF-A compared to laser CNV group (Fig. 2D). Whole membrane images are presented in Fig. S2. These results were confirmed by RCSC flatmount staining of p-IκBα (Fig. 2E); NF-κB downstream proteins COX-2 (Fig. 2F), and VEGF-A (Fig. 2F) were upregulated following laser injury; however, IKK2 Inhibition markedly reduced their expression consistent with WB data.

IKK2 inhibition decreases the infiltration of laser CNV spot with microglia cells and its activation

Double staining of the laser CNV spots with IBA-1 and CD68 (Fig. 3) has revealed the prominent presence of active microglia cells double-positive to IBA-1 and CD68 (Fig. 3A). IKK2 blockade with IMD-0354 has markedly reduced the IBA-1 and CD68 signals restricting them to the CNV spot's center (Fig. 3B).

Infiltration and neovascularization in laser CNV lesions

The strong presence of the GFP positive cells within the laser CNV spots was confirmed by *in vivo* fundus imaging in $Cx3cr1^{gfp/+}$ animals (Fig. 4A), the IMD-0354 treatment reduced the lesion size, infiltration, and GFP intensity (Fig. 4B). These observations were further supported by *ex vivo* microscopy of RCSC flat mounts from $Cx3cr1^{gfp/+}$ mice. In the vehicle-treated eyes, GFP-positive cells migrated to the laser spot; GSA (*Griffonia simplicifolia* agglutinin) lectin staining indicated the presence of endothelial cells within the

area of the highest density of GFP-positive signals within the center of the laser spot (Fig. 4C). Mice in the treatment group demonstrated decreased GFP-positive cells infiltration and reduced neovascularization predominantly restricted in the immediate laser burn site (Fig. 4D) with a minimal spread. Surface area quantification indicated significantly reduced GFP-positive cells infiltration (Fig. 4E, $p < 0.001$) and GSA lectin stained endothelial cells (Fig. 4F, $p < 0.05$) in the IMD-0354 treated group compared with the CNV controls.

Lipopolysaccharide treatment promotes NF-κB activation in BV-2 cells

With clear expression in the cytoplasm, minimal nuclear colocalization of NF-κB was observed in the dimethyl sulfoxide (DMSO)-treated controls (Fig. 5A) in vitro. Lipopolysaccharide (LPS) treatment increased NF-κB signals in the cells and promoted nuclear translocation (Fig. 5B). IKK2 Inhibition with 10 and 25 ng/ml IMD-0354 blocked the nuclear translocation of NF-κB effectively in a dose-dependent manner (Fig. 5C,D). Treatment with IMD-0354 unaffected the cytoplasmic NF-κB presence with almost no nuclear NF-κB signals observed (Fig. 5E). Quantitative analysis (Fig. 5F) demonstrated a significant increase of NF-κB–positive nuclei in LPS–treated BV-2 cells ($p < 0.001$) and the significant inhibitory effect of 10 ng/ml ($p < 0.001$) and 25 ng/ml ($p < 0.001$) IMD-0354 treatment when compared with the LPS-treated positive control. In the DMSO-treated negative control, 25 ng/ml IMD-0354 treatment showed no significant difference in the number of NF-κB–positive nuclei in the presence of LPS ($p > 0.05$). There was no significant difference between nuclear colocalization between DMSO-treated negative control and the IMD0354 25 ng/ml treatment group without LPS stimulation ($p > 0.05$). The NF-κB nuclear translocation results were further corroborated by immunodetection of p-IκBα in the same conditions (Fig. 5G)

IKK2 Inhibition reduces the proinflammatory activation and migration of BV-2 cells

Immunohistochemistry analysis (Fig. 6A) showed that LPS treatment strongly upregulated COX-2 expression in the stimulated BV-2 cells. IKK2 blockade inhibited COX-2 activity in BV-2 cells. These results were further validated by RT-PCR (Fig. 5B), where 25 ng/μl IMD-0354 significantly reduced COX-2 gene expression ($p < 0.05$). The blockade of IKK2 also resulted in decreased migration capacity of BV-2 cells (Fig. 6C). Quantitative analysis of the migratory distance by the BV-2 cells (Fig. 6D) indicated a significant effect of the treatment at both 10 and 25 ng/μl compared to the DMSO-treated control, also indicated by the decreased expression and organization of filamentous actin (F-actin) cytoskeleton (Fig. 6E). Consistent with literature reports [23], LPS treatment also significantly decreased the microglia cells' migration capacity (Fig. 6C). However, F-actin staining demonstrates a very different mechanism of this effect (Fig. 6E). Unlike IKK2 inhibition that resulted in a marked decrease in F-actin expression, LPS-stimulation does not affect cytoskeletal fibers' overall expression but affects its polarization and ultrastructural organization. These results suggest that microglia and other inflammatory cells migrate toward the laser injury site in response to CCL2 and other chemokines but get activated under the effects of COX-2, TNFα, Reactive Oxygen Species (ROS), and other cytotoxic factors at the lesion site.

Discussion

Microglial cells, the resident macrophages of the central nervous system, including the retina, have a significant role in neuronal homeostasis [1, 2]. They display a specific shape of small soma with cellular processes and ramified morphology under a surveillance stage and actively survey the surrounding environment [3]. The activation of microglial cells is known to be induced by injury, infection, and disease conditions, such as diabetic retinopathy and AMD [24]. *In vitro* activation of microglia can be induced by exposure to LPS [25]. Toll-like receptor 4 (TLR4) phosphorylation in microglial activation is thought to trigger cytokine synthesis [25], interferon-γ (IFNγ), or amyloid β (Aβ) upregulation [26, 27]. The release of proinflammatory cytokines plays a pivotal role in the induction and maintenance of neuroinflammation and contributes to disease progression in several chronic neurodegenerative diseases [28, 29]. Microglial activation may also have protective effects on the maintenance of retinal integrity [5], contributing positively to retinal degenerative diseases [6]. Chronic activation of these cells is shown to be involved in the pathogenesis of various degenerative retinal diseases, including AMD [7], inherited retinal dystrophies [8], and glaucoma [10]. Therefore, modulation of microglial reactivity is emerging as a promising therapeutic strategy to treat retinal degenerative diseases [11].

It is well known that NF-κB pathway activation in microglia is a common event downstream to the activation of Toll-like receptor 4 (TLR4), hypoxia, and advanced glycation end-products (AGEs) [30]. In animal models of diabetic retinopathy, AGEs activated microglia in a ROS-dependent manner and upregulated TNF-α secretion [31]. Blocking the NF-κB pathway was proposed to be an attractive strategy for therapies of these retinal diseases [18, 32].

Our current study found that inhibition of IKK2 by IMD-0354 caused significant down-regulation of CNV size, vascular leakage, and microglial cell infiltration in the laser-induced retinal damage, mediated through reduced microglia migration and activation. A significant decrease of nuclear translocation of NF-κB results in the suppression of proinflammatory COX-2 and reduced expression of the VEGF-A. While there are reports that activated microglia have higher migration potency associated with their ameboid morphology [4], the scratch assay in LPS treated microglia cells suggested a reduced migration capacity due to disrupted polarization of the F-actin fibers. Combined with the findings of others, [23] these results suggest that microglia first migrate to the lesion and activate on-site; the *in vitro* findings' applicability to the *in vivo* situation requires further study using the cell tracing. The graphical summary of the findings presented in Fig. 7.

The involvement of IKK2/NF-κB signaling in the development of the laser CNV is well known [33–35]. Lu et al. have elegantly demonstrated the reduction of the laser CNV spots and VEGF-A expression in $IKK2^{-/flox}$:$Nestin^{Cre}$ mice produced through breeding $IKK2^{-/flox}$ animals with $Nestin^{Cre}$ mice [35]. Interestingly, Lu et al. was predominantly focused on RPE in their work. However, a later study by Krishnasamy et al. revealed nestin expression in microglia, especially during proinflammatory insults [36], suggestive that the findings of Lu et al. may also be attributed to the effects of IKK2 inhibition in microglia, which would be consistent with our data.

So far, several compounds with activity against IKK2 have been characterized and demonstrated their promising efficacy in pre-clinical models of several inflammatory diseases [37, 38]. However, despite the promising pre-clinical results from these IKKβ inhibitors, there are many difficulties in adopting them for clinical use. One of the reasons is that IKKβ is ubiquitously expressed and involved in many critical physiological roles [39]. In addition, a suitable targeted delivery approach of the IKK inhibitors should be required to avoid unfavorable side effects [39]. In the eye, topical and local administration remains an option that potentially can mitigate the reported adverse effects of the systemic inhibition of NF-κB signaling. Such as the report by Gaddipati et al., where microparticles loaded with TPCA-1, which is another potent and selective inhibitor of IKK2, ameliorated laser CNV sport formation and proinflammatory signaling without systemic effects or toxicity [35]. Our study demonstrated a subconjunctival injection of IMD-0354 as a potential route of IKK2 inhibitor delivery that allows the use of a small dosage with minimal to no systemic effects while providing sufficient therapeutic concentrations in the eye.

For systemic modulation of NF-κB activation, edasalonexent (CAT-1004), one of the promising new substances with reported selective NF-κB inhibition activity and oral application [40]. Edasalonexent has reached phase 3 clinical trials for Duchenne Muscular Dystrophy (NCT03703882) with no serious complications reported. The potential of edasalonexent in ocular inflammatory conditions and retinal degenerative diseases remains to be elucidated.

Statements of limitation:

1. While Cx3cr1 shows the strongest expression in microglia than other immune cell types, Cx3cr1 is present in microglia, macrophages, and monocytes' subpopulations. [41] Thus, as shown in Fig. 4, we cannot definitively distinguish whether microglial cells or other Cx3cr1-positive cells may migrate towards the laser burn area by disrupting Bruch's membrane [42]. However, the IBA-1 and CD68 staining in WT mice indicate the positive microglia cells (Fig. 2A; Fig 3A) and its reduction in IMD-0354 treated eyes (Fig. 2B; Fig 3B).
2. The $Cx3cr1^{gfp/+}$ mice have one of the copies of the Cx3cr1 gene replaced with the GFP sequence, thus effectively rendering them $Cx3cr1^{-/+}$ animals with the reduced expression of Cx3cr1. Reduced activity of the Cx3cr1 axis may contribute to the more prominent microglial activation [49], and the potentially more intensive proinflammatory response to laser CNV presented in Fig. 4.
3. BV-2 cell is a mouse brain-derived microglial cell line. BV-2 cells represent many microglia cell properties relevant to this work, such as the capacity to become activated in response to LPS stimuli; however, they have unavoidable differences from primary retinal microglia cells.

Conclusion

We demonstrated microglial involvement in the inflammatory and neovascularization signaling in laser CNV and as the potential therapeutic target. Other retinal cells, including retinal pigment epithelium cells and macrophages, have also been suggested in the

pathogenesis of CNV. Since IMD-0354 should beneficially affect NF-κB signaling in these cells and in retinal microglia, investigation of the synergistic effects among microglia, RPE, and other retinal cell types are currently underway.

Materials and methods

Mouse housing, breeding, and genotyping

We used mice for experimentation in accordance with the approved protocols by the University of Missouri Institutional Animal Care and Use Committee (Protocol number: 9520) and performed in accordance with the "Statement for the Use of Animals in Ophthalmic and Vision Research" of the Association for Research in Vision and Ophthalmology (ARVO). Cx3cr1 $^{gfp/gfp}$, C57BL/6J, and Cx3cr1$^{gfp/+}$ mice (The Jackson Laboratory, Bar Harbor, ME, USA) were housed at the pathogen-free animal facilities of the Bone Life Sciences Center at the University of Missouri and were fed normal chow diets and provided with water *ad libitum* under 12-hour light-dark cycles. Cx3cr1$^{gfp/+}$ mice were produced by breeding Cx3cr1$^{gfp/gfp}$ males with C57BL/6J female mice. Genomic DNA (gDNA) was extracted from tail tip material (approximately 1–2 mm in length) from C57BL/6J mice and was analyzed, with assistance from Transnetyx (www.transnetyx.com, Cordova, TN, USA), for the presence of the Cx3cr1-GFP insert.

C57BL/6 mice for additional experiments at Sapporo Medical University were obtained from Hokudo (Sapporo, Japan) and bred in a pathogen-free condition at the Sapporo Medical University Animal Resource Center. The study protocol was approved by the Sapporo Medical University School of Medicine Ethics Committee.

Laser CNV induction and subconjunctival injection of IMD-0354

The laser CNV model was performed according to previously published procedures. [4] Here, 6~8-week-old C57BL/6J and Cx3cr1$^{gfp/wt}$ mice were used for the study. Briefly, the mice were anesthetized with ketamine hydrochloride (100 mg/kg body weight) and xylazine (4 mg/kg body weight), and the pupils were dilated with 1% tropicamide. Laser injury (75-μm spot size, 0.1-second duration, 120 mW) was induced in the 9, 12, and 3 o'clock positions of the posterior pole of the retina with the slit-lamp delivery system of an OcuLight GL diode laser (Iridex, Mountain View, CA, USA) and a handheld plastic cover as a contact lens to view the retina. Only burns in which a bubble was produced were used in the study.

IMD-0354 and preparation of experimental solutions—IMD-0354 (I3159, Sigma, St. Louis, MO, USA) was dissolved in dimethylsulfoxide (DMSO; Sigma, St. Louis, MO, USA) to produce a 10 mg/ml stock solution. For animal injection, the stock solution was then further dissolved in (0.5% sodium carboxymethylcellulose solution (CMC) diluted in PBS; Sigma, St. Louis, MO, USA) to produce 1 μg/μl concentration, and animals were delivered 10 μl (10 μg) subconjunctivally. For the cell treatment, the stock solution was dissolved in pure DMSO to 10 ng/μl concentration. For systemic application, mice received daily doses of IMD-0354 (100 μl, intraperitoneally, 30 mg/kg) suspended in (0.5% sodium carboxymethylcellulose solution (CMC, Sigma, St. Louis, MO, USA) diluted in PBS or vehicle CMC (100 μl, intraperitoneally).

Fundus examination and fluorescein angiography under retinal-imaging microscopy

Five days after induction of Laser CNV, Mice were anesthetized intraperitoneally with Ketanest (ketamine; 25 mg/ml, 0.4 ml, Pfizer, New York, NY, USA) and Dexdomitor (dexmedetomidine hydrochloride; 0.5 mg/ml, 0.2 ml, Orion Pharma, Hamburg, Germany). The pupils were dilated with 1% tropicamide (Sandoz, West Princeton, NJ, US). The cornea was protected with hypromellose ophthalmic demulcent solution (Gonak 2.5%, Akorn L.L.C., Akron, OH, USA), a transparent gonioscopy gel. The fundus examination was performed with a MICRON III retinal imaging microscope (Phoenix Research Labs, Inc., Pleasanton, CA, USA). Fundus vascular fluorescence was observed using 488-nm excitation with a 520-nm emission filter. Fluorescent angiographies were taken 120 seconds after subcutaneous injection of fluorescein sodium (250 μl, 100 mg/ml). GFP-positive cells infiltration in Cx3cr1$^{gfp/wt}$ mice was observed using 488-nm excitation with a 520-nm emission filter.

RCSC flat mounts

The eyeballs were collected 5 days after laser exposure and fixed with 4% paraformaldehyde (Sigma, St. Louis, MO, USA) for 12 hours. Under an Olympus SZ-STB1 dissection microscope (Olympus, Tokyo, Japan), the anterior segment tissues, vitreous, and retinas were removed to isolate the RCSC. Approximately 4–8 relaxing radial incisions were made. The remaining RCSC were incubated in a blocking solution of 5% normal goat serum (NGS) (Thermo Fisher Scientific, Waltham, MA, USA) with 0.01% Triton-X (Sigma, St. Louis, MO, USA) overnight. The RCSC was then incubated with antibodies against IBA-1, NF-κB, COX-2, p-IκBα, and VEGF-A (Table 1) for 24 hours, followed by washing three times for 30 minutes with PBS-T. Then, the samples were incubated for 24 hours with anti-rabbit and anti-mouse Alexa Flour 647 and 488 (1:1000; Thermo Fisher Scientific, Waltham, MA, USA). GSA-lectin staining was performed by incubation of the blocked flatmounts with Isolectin GS-IB4 From Griffonia simplicifolia, Alexa Fluor™ 647 Conjugate (1:100; I32450; Thermo Fisher Scientific, Waltham, MA, USA) overnight 4C. Following PBS-T washing, the samples were counterstained with DAPI (1:5000; Sigma, St. Louis, MO, USA) and mounted using ProLong Diamond antifade reagent (Thermo Fisher Scientific, Waltham, MA, USA). The laser CNV lesion site's surface area was determined by the RPE disruption area visualized by *in vivo* injection of fluorescein with *ex vivo* DAPI counterstaining. The size of endothelial and inflammatory cells infiltration (GSA-lectin positive) and in Cx3cr1$^{gfp/wt}$ animals by the GFP-positive cells. The surface area was determined using ImageJ (https://imagej.nih.gov/ij/) by determining the pixel number in the selected area and dividing it to the pixel number in 100 μm^2 square produced from the scale bar: (pixel number in the area/pixel number in 100 μm^2 square)*100=surface area in μm^2 as reported previously. [43]

Western blotting—Western Blotting (WB) was performed as previously described with some modifications [44, 45]. RCSC were isolated on ice and sonicated in a cold radioimmunoprecipitation assay (RIPA) buffer containing FAST protease inhibitors (Cat#: S8830, Sigma, St. Louis, MO, USA). The protein concentration was determined using a Qubit 4 fluorometer (Thermo Fisher Scientific, Waltham, MA, USA). Before the electrophoretic transfer to 0.45 μm pore-size nitrocellulose membranes, 30 μg total protein

per lane was separated by sodium dodecyl sulfate-polyacrylamide gel electrophoresis (4–20% polyacrylamide gel). The protein sizes were resolved by running 10 μl of ExcelBand™ 3-color Regular Range Protein Marker (PM2500, SMOBIO Technology, Inc., Hsinchu City, Taiwan). The membranes were blocked with 5% BSA (A7096) at RT for 1 h and then incubated overnight at 4°C with the primary antibod ies (Table 1). After being washed with a PBS-T buffer, the blots were incubated with an HRP-conjugated secondary antibody (1:1000; Bio-Rad Laboratories, Hercules, CA, USA) for 1 h at RT. The signals were developed with enhanced chemiluminescence with a SuperSignal West Pico kit (Thermo Fisher Scientific, Waltham, MA, USA) and detected with an ImageQuant LAS 500 (GE Healthcare, Chicago, IL, USA).

Cells and culture conditions

The immortalized mouse microglia line BV-2 (EOC 20; CRL-2469; Lot 70005904; American Type Culture Collection, ATCC, Manassas, VA, USA), derived from the C3H/HeJ female mouse, was used at passage 7. BV-2 cells were maintained in Dulbecco's modified Eagle's medium (DMEM, Thermo Fisher Scientific, Waltham, MA, USA) and supplemented with 10% fetal bovine serum (FBS, Thermo Fisher Scientific, Waltham, MA, USA), 1% penicillin/streptomycin (Pen/Strep, Thermo Fisher Scientific, Waltham, MA, USA), and 20% LADMAC conditioned medium (LCM). Mouse bone marrow-derived from the macrophage cell line LADMAC (CRL-2420; Lot 63407846; ATCC) was used as a source of crude CSF-1 (colony-stimulating factor 1) to supplement BV-2 cell growth. LADMAC cells were grown to confluence in complete DMEM; then, the medium was changed to fresh complete DMEM; 24 hours later, the conditioned medium was collected and centrifuged at 5000 ×*g* for 10 minutes to remove cells and debris, resulting in supernatant that was filtered through a Target2™ 0.2-μm pore size, syringe-driven filter (F2513–2, Thermo Fisher Scientific, Waltham, MA, USA). The resulting LCM was stored at −20°C until use. In the experiments involving LPS stimulation of BV-2 cells, the BV-2 cells were grown for 12 hours in an FBS-free medium (DMEM, 1% Pen/Strep).

Imaging

Fluorescent images of flat mounts and cells were acquired with an LSM 700 laser confocal microscope (Carl Zeiss, Oberkochen, Germany) and Leica SP8 (Leica Camera AG, Wetzlar, Germany). Calcein acetoxymethyl ester (calcein-AM)-stained BV-2 cell migration data were acquired using the EVOS FLc imaging system (Thermo Fisher Scientific, Waltham, MA, USA).

Immunohistochemistry

BV-2 cells were seeded at 5×10^3 cells per well in Millicell EZ slides (Millipore, Billerica, MA, USA) and grown to 80% confluence in LCM After 12-hour serum starvation. The cells were treated with 10 and 25 ng/ml IMD-0354; following 1-hour incubation; the cells were stimulated with 1 μg/ml LPS (Sigma, St. Louis, MO, USA) for 24 hours. The samples were fixed with 1% formaldehyde (Sigma, St. Louis, MO, USA) for 10 minutes, permeabilized by incubation with 0.2% Triton X-100 (Sigma, St. Louis, MO, USA) in phosphate-buffered saline (PBS) for 15 minutes, and then blocked with 5% normal goat serum (NGS) (Thermo Fisher Scientific, Waltham, MA, USA) for 1 hour at room temperature. The samples

were incubated with antibodies against COX-2, p-IκBα (Table 1) overnight; the signals were then visualized using anti-rabbit secondary antibodies DyLight 647 and 488 (1:1000; Thermo Fisher Scientific, Waltham, MA, USA). The sections were counterstained with 4',6-diamidino-2-phenylindole (DAPI, 1:5000; Sigma, St. Louis, MO) and mounted with ProLong Diamond antifade reagent (Thermo Fisher Scientific, Waltham, MA, USA).

F-actin staining

BV-2 cells were grown to 80% confluence as described above and treated with 10 and 25 ng/ml IMD-0354, and incubated for 12 hours. The samples were fixed with 1% formaldehyde (Sigma, St. Louis, MO, USA) for 10 minutes, permeabilized by incubation with 0.2% Triton X-100 (Sigma, St. Louis, MO, USA) in PBS for 15 minutes, and then blocked with 5% NGS (Thermo Fisher Scientific, Waltham, MA, USA) for 1 hour at room temperature. Then, the samples were incubated with phalloidin red (1:100; Thermo Fisher Scientific, Waltham, MA, USA) for 1 hour at room temperature and washed with PBS-Tween 20 (0.05%; PBS-T). Next, the samples were counterstained with DAPI (1:5000; Sigma, St. Louis, MO, USA) and mounted with ProLong Diamond antifade reagent (Thermo Fisher Scientific, Waltham, MA, USA).

BV-2 cell migration assay

BV-2 cells were grown to confluence in a 6-well plate in complete medium with 20% LCM supplementation. A scratch along the diameter of the well was made using a sterile razor blade; the cells were then washed with PBS and covered with complete medium with 20% LCM, and treated with 10 and 25 ng/ml IMD-0354; the controls were DMSO-treated cells. At 96 hours after treatment, the cells were visualized with 1 μg/ml Calcein-AM (C3100MP; Thermo Fisher Scientific, Waltham, MA) and imaged using an EVOS fluorescence microscope (Thermo Fisher Scientific, Waltham, MA, USA) at 488 nm excitation. The start point was determined based on the original imprint of the blade at the bottom of each well. The distance from the starting point to the furthest distance migrated was measured and quantified. Three images were obtained from each well, and the results were averaged.

RNA isolation and quantitative RT-PCR (qRT-PCR)

The cells were washed with PBS, and total RNA was extracted using an RNeasy Plus Mini Kit (Qiagen, Germantown, MD, USA) according to the kit protocol with the addition of Buffer R.L.T. Plus supplemented with 20 μl 2 M dithiothreitol (DTT). The RNA was analyzed for quality and was quantified using a NanoDrop One unit (Thermo Fisher Scientific, Waltham, MA), and reverse-transcribed to complementary DNA (cDNA) using Maxima™ H Minus cDNA Synthesis Master Mix with double-strand–specific DNase (dsDNase, M1682; Thermo Fisher Scientific, Waltham, MA, USA) according to the manufacturer's protocol in a SimpliAmp Thermal Cycler (Life Technologies, Waltham, MA, USA). Gene expression was analyzed using Power SYBR Green Master Mix (Thermo Fisher Scientific, Waltham, MA, USA) with the following mouse-specific primers: COX-2 (forward: GCGAGCTAAGAGCTTCAGGA, reverse: CAGACGCCACTGTCGCTTT) by Sánchez-Miranda et al. [46] and cyclophilin was used as housekeeping gene (forward: CAGACGCCACTGTCGCTTT, reverse: TGTCTTTGGAACTTTGTCTG) Catoire et al.

[47] using QuantStudio 3 real-time PCR (RT-PCR) system (Applied Biosystems, Foster City, CA, USA). The relative expression values of the target genes were normalized to cyclophilin, and the fold change was calculated using the relative quantification (2−ΔΔCT) method. Four biological replicates per treatment group were run in three technical replicates.

Colocalization analysis—The colocalization analysis between DAPI and NF-κB signals was performed using the EzColocalization plug-in for ImageJ [48]. Individual fluorescent channel images were converted to 8-bit grayscale and analyzed using default parameters. Cell identification was set to DAPI.

Statistical analysis

All values were present as the mean ± standard deviation (SD) for the respective groups. Statistical analyses were performed with GraphPad Prism (https://www.graphpad.com/scientific-software/prism/). The Student's *t*-test was used when comparing two groups. A one-way analysis of variance (ANOVA) with Tukey multiple comparisons was used whenever comparing multiple groups. A p-value of <0.05 was considered significant. The figures use the following designations for the p-value: not significant (n.s.), $p > 0.05$; * $p < 0.05$; ** $p < 0.01$; *** $p < 0.001$.

Supplementary Material

Refer to Web version on PubMed Central for supplementary material.

Acknowledgments

The authors would like to acknowledge the contribution of TransnetYX for assisting with the probe design and animal genotyping; Ms. Lijuan Fan (Department of Ophthalmology, University of Missouri School of Medicine, Columbia, Missouri) for benchwork assistance. Ms. Catherine Brooks J. (Department of Ophthalmology, University of Missouri School of Medicine, Columbia, Missouri) for benchwork assistance and language corrections. Confocal images in part were acquired at the University of Missouri Molecular Cytology Core facility. Mr. Dmitry Rumyancev (Belgorod, Russia) for graphical abstract artwork design.

Funding

This work was supported in part by the Northern Advances Center for Science & Technology (NOASTEC) Foundation (Anton Lennikov); NIH grant R01 EY027824 (Hu Huang); Missouri University startup funds (Hu Huang).

References

[1]. Jager RD, Mieler WF, Miller JW, Age-related macular degeneration NEngl J Med358 (2008) 2606–2617.

[2]. Ip MS, Scott IU, Brown GC, Brown MM, Ho AC, Huang SS, Recchia FM, American Academy of O, Anti-vascular endothelial growth factor pharmacotherapy for age-related macular degeneration: a report by the American Academy of Ophthalmology, Ophthalmology115 (2008) 1837–1846. [PubMed: 18929163]

[3]. Murakami Y, Ikeda Y, Yonemitsu Y, Miyazaki M, Inoue M, Hasegawa M, Sueishi K, Ishibashi T, Inhibition of choroidal neovascularization via brief subretinal exposure to a newly developed lentiviral vector pseudotyped with Sendai viral envelope proteins, Hum Gene Ther21 (2010) 199–209. [PubMed: 19778186]

[4]. Saint-Geniez M, Kurihara T, Sekiyama E, Maldonado AE, D'Amore PA, An essential role for RPE-derived soluble VEGF in the maintenance of the choriocapillaris, Proc Natl Acad Sci U S A106 (2009) 18751–18756.

[5]. Moorthy S, Cheung N, Cerebrovascular accidents and ranibizumab, Ophthalmology116 (2009) 1834–1835; author reply 1835. [PubMed: 19729107]

[6]. Ueta T, Yanagi Y, Tamaki Y, Yamaguchi T, Cerebrovascular accidents in ranibizumab, Ophthalmology116 (2009) 362.

[7]. Sniegowski M, Mandava N, Kahook MY, Sustained intraocular pressure elevation after intravitreal injection of bevacizumab and ranibizumab associated with trabeculitis, Open Ophthalmol J4 (2010) 28–29. [PubMed: 20871754]

[8]. Bakri SJ, Larson TA, Edwards AO, Intraocular inflammation following intravitreal injection of bevacizumab, Graefes Arch Clin Exp Ophthalmol246 (2008) 779–781. [PubMed: 18204851]

[9]. Yang S, Zhao J, Sun X, Resistance to anti-VEGF therapy in neovascular age-related macular degeneration: a comprehensive review, Drug Des Devel Ther10 (2016) 1857–1867.

[10]. Nagai N, Izumi-Nagai K, Oike Y, Koto T, Satofuka S, Ozawa Y, Yamashiro K, Inoue M, Tsubota K, Umezawa K, Ishida S, Suppression of diabetes-induced retinal inflammation by blocking the angiotensin II type 1 receptor or its downstream nuclear factor-kappaB pathway, Invest Ophthalmol Vis Sci48 (2007) 4342–4350. [PubMed: 17724226]

[11]. Chen ZJ, Ubiquitin signalling in the NF-kappaB pathway, Nat Cell Biol7 (2005) 758–765. [PubMed: 16056267]

[12]. Cahir-McFarland ED, Carter K, Rosenwald A, Giltnane JM, Henrickson SE, Staudt LM, Kieff E, Role of NF-kappa B in cell survival and transcription of latent membrane protein 1-expressing or Epstein-Barr virus latency III-infected cells, J Virol78 (2004) 4108–4119. [PubMed: 15047827]

[13]. Saddala MS, Lennikov A, Mukwaya A, Yang Y, Hill MA, Lagali N, Huang H, Discovery of novel L-type voltage-gated calcium channel blockers and application for the prevention of inflammation and angiogenesis, J Neuroinflammation17 (2020) 132. [PubMed: 32334630]

[14]. Inayama M, Nishioka Y, Azuma M, Muto S, Aono Y, Makino H, Tani K, Uehara H, Izumi K, Itai A, Sone S, A novel IkappaB kinase-beta inhibitor ameliorates bleomycin-induced pulmonary fibrosis in mice, Am J Respir Crit Care Med173 (2006) 1016–1022. [PubMed: 16456147]

[15]. Onai Y, Suzuki J, Kakuta T, Maejima Y, Haraguchi G, Fukasawa H, Muto S, Itai A, Isobe M, Inhibition of IkappaB phosphorylation in cardiomyocytes attenuates myocardial ischemia/reperfusion injury, Cardiovasc Res63 (2004) 51–59. [PubMed: 15194461]

[16]. Sugita A, Ogawa H, Azuma M, Muto S, Honjo A, Yanagawa H, Nishioka Y, Tani K, Itai A, Sone S, Antiallergic and anti-inflammatory effects of a novel I kappaB kinase beta inhibitor, IMD-0354, in a mouse model of allergic inflammation, Int Arch Allergy Immunol148 (2009) 186–198. [PubMed: 18849610]

[17]. Kamon J, Yamauchi T, Muto S, Takekawa S, Ito Y, Hada Y, Ogawa W, Itai A, Kasuga M, Tobe K, Kadowaki T, A novel IKKbeta inhibitor stimulates adiponectin levels and ameliorates obesity-linked insulin resistance, Biochem Biophys Res Commun323 (2004) 242–248. [PubMed: 15351728]

[18]. Lennikov A, Kitaichi N, Noda K, Ando R, Dong Z, Fukuhara J, Kinoshita S, Namba K, Mizutani M, Fujikawa T, Itai A, Ohno S, Ishida S, Amelioration of endotoxin-induced uveitis treated with an IkappaB kinase beta inhibitor in rats, Mol Vis18 (2012) 2586–2597. [PubMed: 23112571]

[19]. Lasemi N, Bomati Miguel O, Lahoz R, Lennikov VV, Pacher U, Rentenberger C, Kautek W, Laser-Assisted Synthesis of Colloidal FeWx Oy and Fe/Fex Oy Nanoparticles in Water and Ethanol, Chemphyschem19 (2018) 1414–1419. [PubMed: 29543395]

[20]. Haddock LJ, Kim DY, Mukai S, Simple, inexpensive technique for high-quality smartphone fundus photography in human and animal eyes, J Ophthalmol2013 (2013) 518479.

[21]. Jung S, Aliberti J, Graemmel P, Sunshine MJ, Kreutzberg GW, Sher A, Littman DR, Analysis of fractalkine receptor CX(3)CR1 function by targeted deletion and green fluorescent protein reporter gene insertion, Mol Cell Biol20 (2000) 4106–4114. [PubMed: 10805752]

[22]. Huang H, Parlier R, Shen JK, Lutty GA, Vinores SA, VEGF receptor blockade markedly reduces retinal microglia/macrophage infiltration into laser-induced CNV, PLoS One8 (2013) e71808.

[23]. Lively S, Schlichter LC, The microglial activation state regulates migration and roles of matrix-dissolving enzymes for invasion, J Neuroinflammation10 (2013) 75. [PubMed: 23786632]

[24]. Rashid K, Akhtar-Schaefer I, Langmann T, Microglia in Retinal Degeneration, Frontiers in immunology10 (2019) 1975. [PubMed: 31481963]

[25]. Hanisch D, Zimmer R, Lengauer T, ProML--the protein markup language for specification of protein sequences, structures and families, In Silico Biol2 (2002) 313–324. [PubMed: 12542416]

[26]. Lacy P, Stow JL, Cytokine release from innate immune cells: association with diverse membrane trafficking pathways, Blood118 (2011) 9–18. [PubMed: 21562044]

[27]. Giulian D, Li J, Leara B, Keenen C, Phagocytic microglia release cytokines and cytotoxins that regulate the survival of astrocytes and neurons in culture, Neurochem Int25 (1994) 227–233. [PubMed: 7833791]

[28]. Smith GS, Voyer-Grant JA, Harauz G, Monitoring cleaved caspase-3 activity and apoptosis of immortalized oligodendroglial cells using live-cell imaging and cleaveable fluorogenic-dye substrates following potassium-induced membrane depolarization, J Vis Exp (2012).

[29]. Zheng C, Zhou XW, Wang JZ, The dual roles of cytokines in Alzheimer's disease: update on interleukins, TNF-alpha, TGF-beta and IFN-gamma, Transl Neurodegener5 (2016) 7. [PubMed: 27054030]

[30]. Sung IS, Park SY, Jeong KY, Kim HM, Investigation of the preventive effect of calcium on inflammation-mediated choroidal neovascularization, Life Sci233 (2019) 116727.

[31]. Bonfigli A, Colafarina S, Falone S, Di Giulio C, Di Ilio C, Amicarelli F, High levels of antioxidant enzymatic defence assure good protection against hypoxic stress in spontaneously diabetic rats, Int J Biochem Cell Biol38 (2006) 2196–2208. [PubMed: 16904932]

[32]. Lennikov A, Hiraoka M, Abe A, Ohno S, Fujikawa T, Itai A, Ohguro H, IkappaB kinase-beta inhibitor IMD-0354 beneficially suppresses retinal vascular permeability in streptozotocin-induced diabetic mice, Invest Ophthalmol Vis Sci55 (2014) 6365–6373. [PubMed: 25205865]

[33]. Martinez B, Peplow P, MicroRNAs in laser-induced choroidal neovascularization in mice and rats: their expression and potential therapeutic targets, Neural Regeneration Research16 (2021) 621–627. [PubMed: 33063711]

[34]. Wang H, Kunz E, Stoddard GJ, Hauswirth WW, Hartnett ME, Optimal Inhibition of Choroidal Neovascularization by scAAV2 with VMD2 Promoter-driven Active Rap1a in the RPE, Scientific Reports9 (2019) 15732.

[35]. Gaddipati S, Lu Q, Kasetti RB, Miller MC, Lu Q, Trent JO, Kaplan HJ, Li Q, IKK2 inhibition using TPCA-1-loaded PLGA microparticles attenuates laser-induced choroidal neovascularization and macrophage recruitment, PLoS One10 (2015) e0121185.

[36]. Krishnasamy S, Weng Y-C, Thammisetty SS, Phaneuf D, Lalancette-Hebert M, Kriz J, Molecular imaging of nestin in neuroinflammatory conditions reveals marked signal induction in activated microglia, Journal of Neuroinflammation14 (2017) 45. [PubMed: 28253906]

[37]. Kobori M, Yang Z, Gong D, Heissmeyer V, Zhu H, Jung YK, Gakidis MA, Rao A, Sekine T, Ikegami F, Yuan C, Yuan J, Wedelolactone suppresses LPS-induced caspase-11 expression by directly inhibiting the IKK complex, Cell Death Differ11 (2004) 123–130. [PubMed: 14526390]

[38]. Nam NH, Naturally occurring NF-kappaB inhibitors, Mini Rev Med Chem6 (2006) 945–951. [PubMed: 16918500]

[39]. Prescott JA, Cook SJ, Targeting IKKbeta in Cancer: Challenges and Opportunities for the Therapeutic Utilisation of IKKbeta Inhibitors, Cells7 (2018).

[40]. Donovan JM, Zimmer M, Offman E, Grant T, Jirousek M, A Novel NF-kappaB Inhibitor, Edasalonexent (CAT-1004), in Development as a Disease-Modifying Treatment for Patients With Duchenne Muscular Dystrophy: Phase 1 Safety, Pharmacokinetics, and Pharmacodynamics in Adult Subjects, J Clin Pharmacol57 (2017) 627–639. [PubMed: 28074489]

[41]. Burgess M, Wicks K, Gardasevic M, Mace KA, Cx3CR1 Expression Identifies Distinct Macrophage Populations That Contribute Differentially to Inflammation and Repair, Immunohorizons3 (2019) 262–273. [PubMed: 31356156]

[42]. Lee M, Lee Y, Song J, Lee J, Chang SY, Tissue-specific Role of CX3CR1 Expressing Immune Cells and Their Relationships with Human Disease, Immune Netw18 (2018) e5.

[43]. Saddala MS, Lennikov A, Mukwaya A, Huang H, Transcriptome-Wide Analysis of CXCR5 Deficient Retinal Pigment Epithelial (RPE) Cells Reveals Molecular Signatures of RPE Homeostasis, Biomedicines8 (2020).

[44]. Huang H, Shen J, Vinores SA, Blockade of VEGFR1 and 2 suppresses pathological angiogenesis and vascular leakage in the eye, PLoS One6 (2011) e21411.

[45]. Huang H, Van de Veire S, Dalal M, Parlier R, Semba RD, Carmeliet P, Vinores SA, Reduced retinal neovascularization, vascular permeability, and apoptosis in ischemic retinopathy in the absence of prolyl hydroxylase-1 due to the prevention of hyperoxia-induced vascular obliteration, Investigative ophthalmology & visual science52 (2011) 7565–7573. [PubMed: 21873682]

[46]. Sanchez-Miranda E, Lemus-Bautista J, Perez S, Perez-Ramos J, Effect of kramecyne on the inflammatory response in lipopolysaccharide-stimulated peritoneal macrophages, Evid Based Complement Alternat Med2013 (2013) 762020.

[47]. Catoire M, Alex S, Paraskevopulos N, Mattijssen F, Evers-van Gogh I, Schaart G, Jeppesen J, Kneppers A, Mensink M, Voshol PJ, Olivecrona G, Tan NS, Hesselink MK, Berbee JF, Rensen PC, Kalkhoven E, Schrauwen P, Kersten S, Fatty acid-inducible ANGPTL4 governs lipid metabolic response to exercise, Proc Natl Acad Sci U S A111 (2014) E1043–1052.

[48]. Stauffer W, Sheng H, Lim HN, EzColocalization: An ImageJ plugin for visualizing and measuring colocalization in cells and organisms, Scientific reports8 (2018) 15764.

Highlights

- IMD0354 treatment caused a significant reduction in the fluorescein leakage and size of the laser CNV spots and microglia infiltration

- IKK2 inhibition suppressed phospho-IκBα, VEGF-A, and COX-2 in the Laser CNV mouse eyes.

- IMD-0354 treated eyes demonstrated reduced microglial migration to the laser injury site.

- *In vitro*, IKK2 inhibition reduced NF-κB activation, COX-2, Actin-F presence, and the microglia cells' migration capacity.

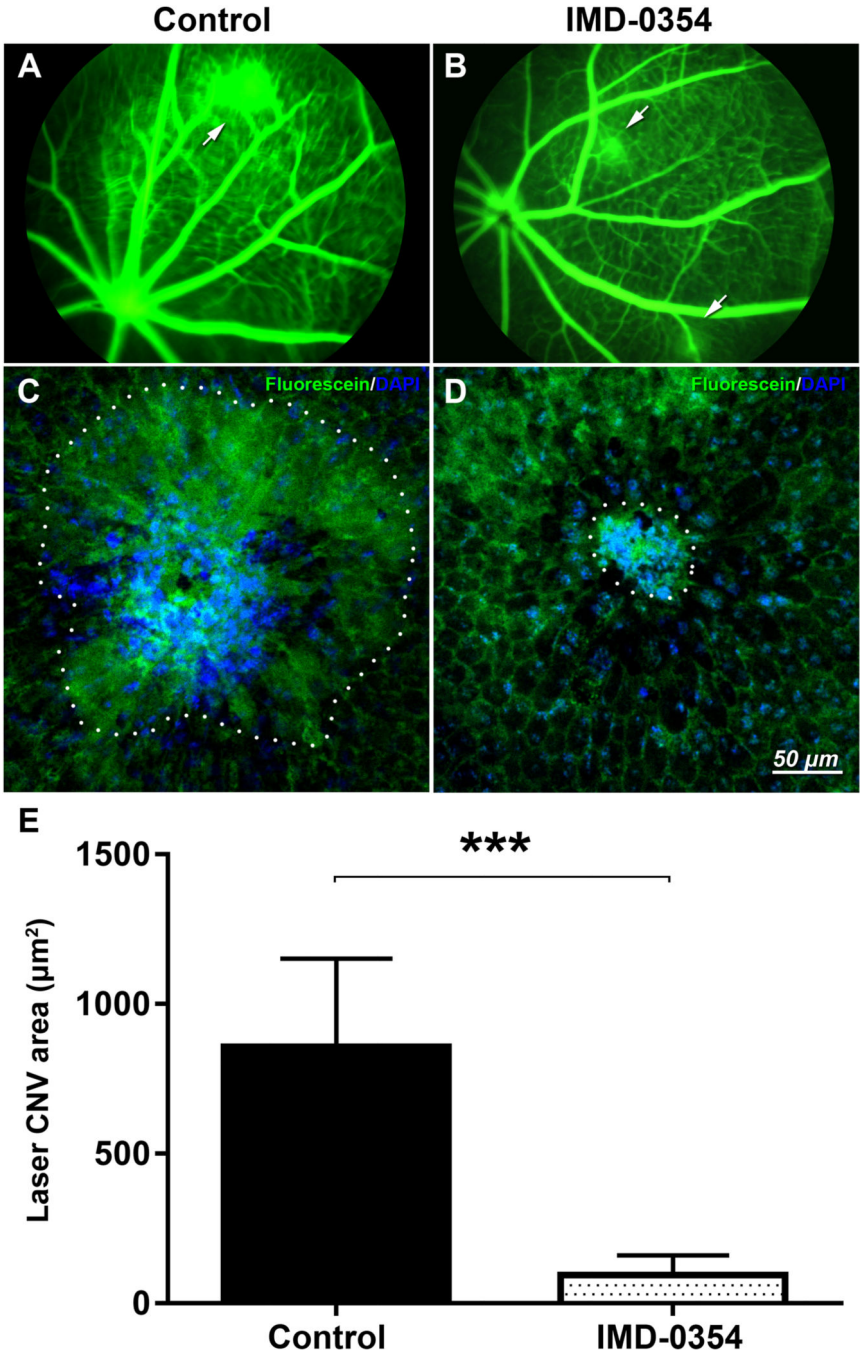

Figure 1:

Effects of IKK2 Inhibition on laser-induced CNV in mice.

In vivo fluorescent angiography in control animals (**A**) or animals treated with subconjunctival IMD-0354 (10 μg) (**B**) 5 days after laser CNV induction. Images were taken 60 seconds after the subcutaneous injection of fluorescein sodium. Arrows indicate fluorescein leakage areas. *Ex vivo* evaluation of the laser spot sizes in RCSC flat mounts in control (**C**) and IMD-0354-treated eyes (**D**). Quantitative analysis of laser CNV area in

RCSC flat mounts (**E**). Statistical significance was determined using Student's *t*-test. ***p < 0.001. n=5 (5 eyes, 15 CNV spots)

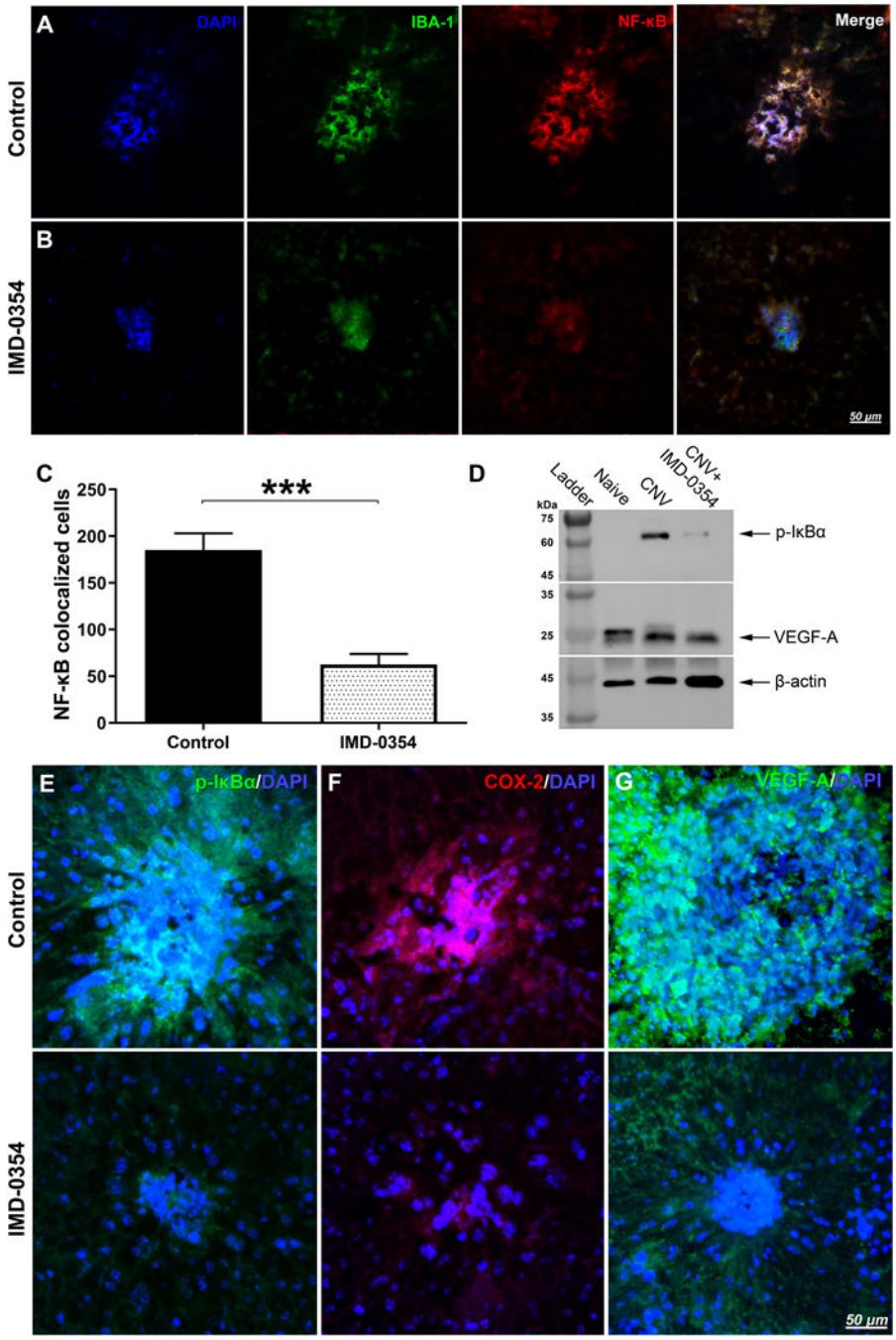

Figure 2:

Immunofluorescent evaluation of NF-κB activation and NF-κB downstream signaling protein expression within the laser spots with and without IKK2 Inhibition in RCSC flat mounts.

Effect of IKK2 Inhibition on the presence of IBA-1 positive microglial cells (green) with NF-κB (red) nuclear (blue) translocation within the laser spot in mouse RCSC 5 days after laser CNV induction. The vesicle-treated controls **(A)** and eyes were treated with subconjunctival IMD-0354 (10 μg) (**B**). Quantitative analysis of NF-κB colocalized cells.

Representative images of NF-κB/DAPI double staining and colocalization are present in Fig. S1A-B. (**C**). Statistical significance was determined using Student's *t*-test. ***$p < 0.001$. n=6 (6 eyes, 18 CNV spots) (**D**) Western blot analysis of p-IκBα and VEGF-A in RCSC lysates of Naïve controls, laser CNV control, and IMD-0354 treated animals. β-actin was used as the loading control. Full-length blots are presented in Fig. S2. Immunofluorescence evaluation of p-IκBα (**E**), COX-2 (**F**), VEGF-A (**G**) within laser spots in mouse RCSC with and without IKK2 inhibition 5 days after laser CNV induction.

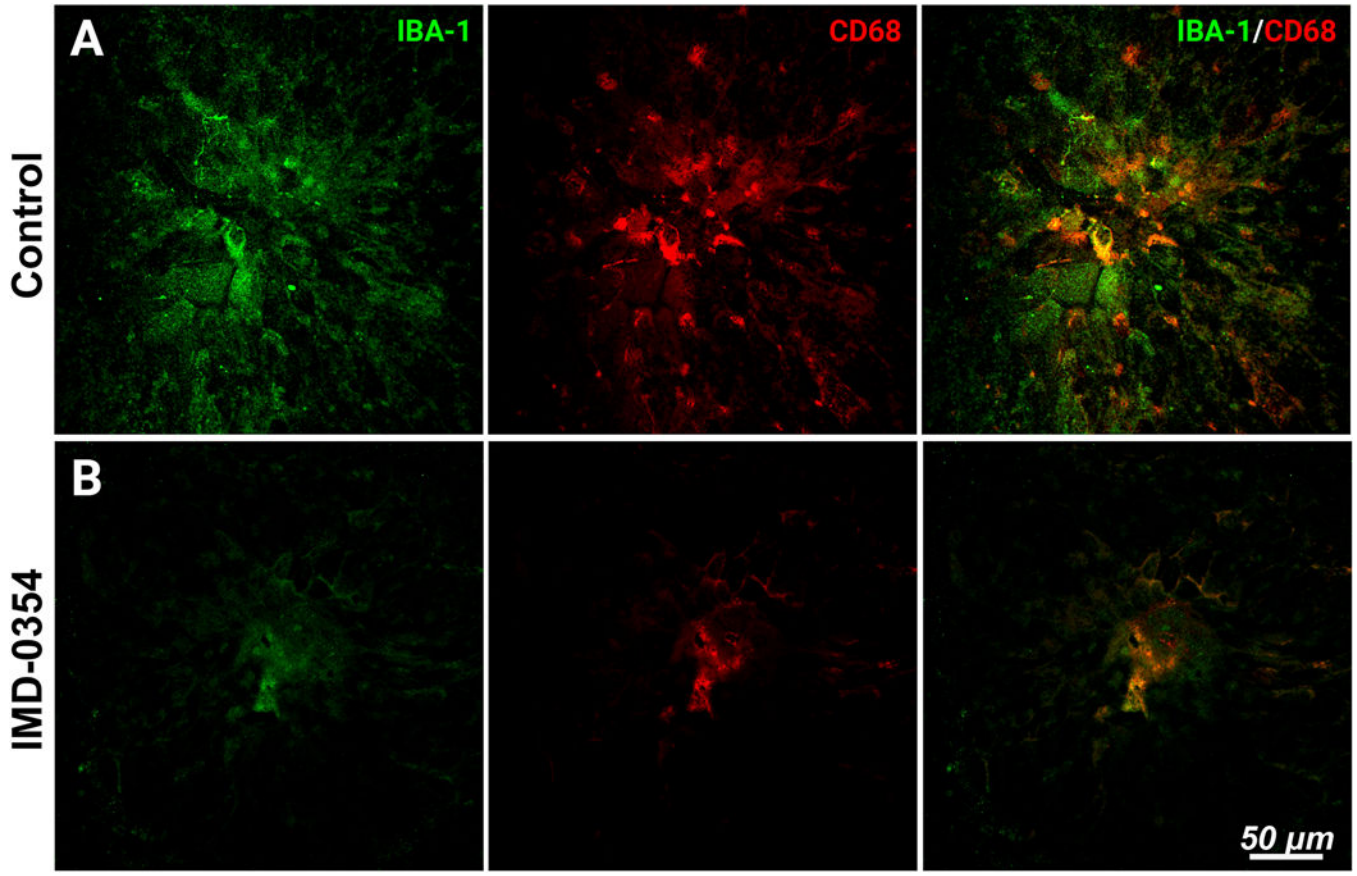

Figure 3:

Microglia infiltration and activation within the laser CNV spot with and without IKK2 inhibition.

IBA-1 and CD68 staining of the laser CNV spot in control (**A**); and IMD-0354 treated mice (**B**).

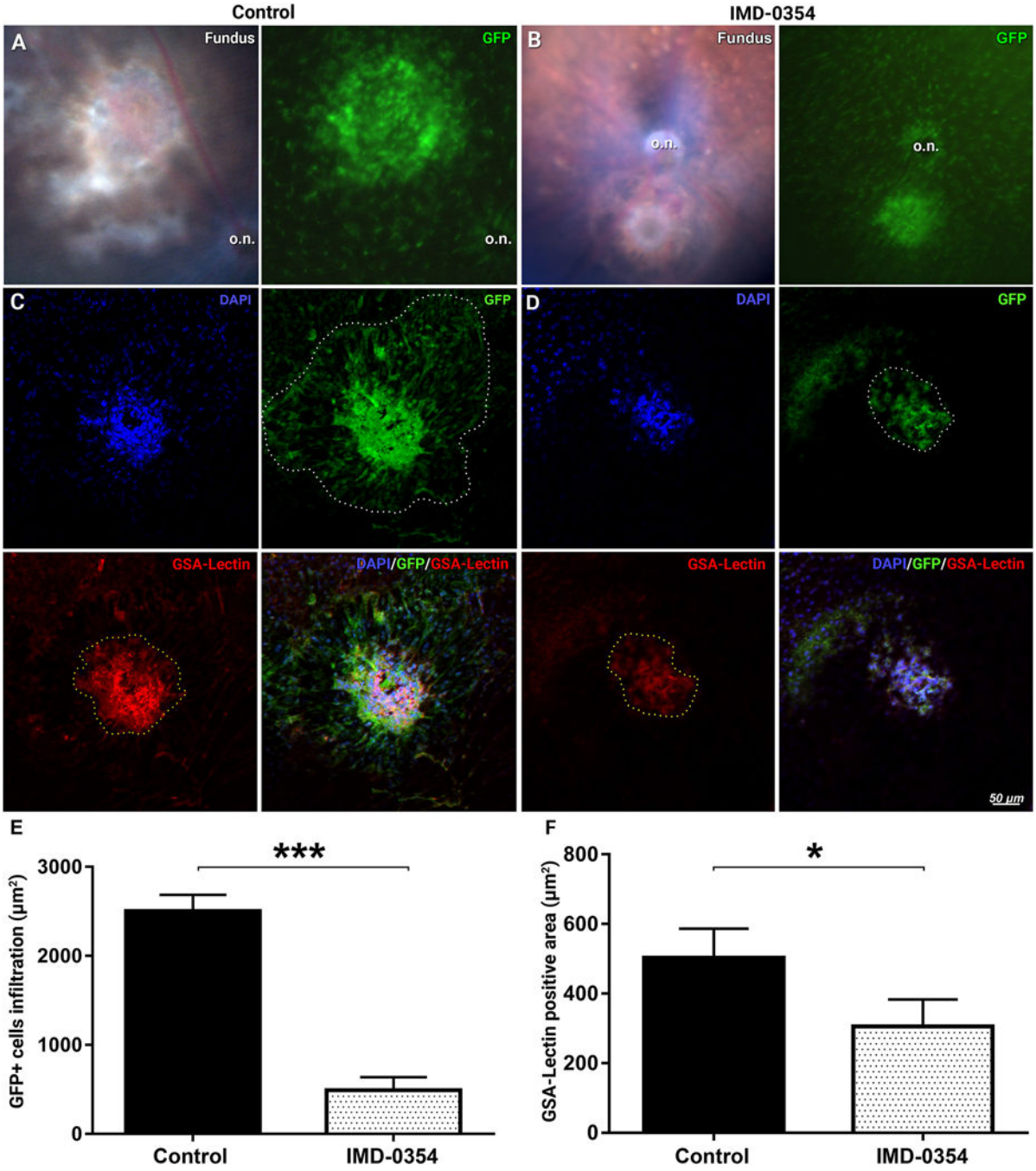

Figure 4:

Dynamic of retinal microglial cells and neovascularization in laser CNV model in Cx3cr1$^{gfp/+}$ mice with and without IKK2 inhibition.

Visible light and 488 nm fluorescent fundus images of laser CNV control (**A**) and IMD-0354 treated animals (**B**). o.n –indicate optic nerve disk. Infiltration with GFP-positive microglial cells of the laser CNV spot and GSA lectin–positive neovessels in the vesicle treated controls (**C**) or eyes treated with subconjunctival IMD-0354 (10 μg) (**D**) 5 days after model induction. Quantitative analysis of GFP-positive cells infiltration (**E**) and GSA lectin–stained

neovascularization areas surface (**F**). Statistical significance was determined using Student's *t*-test. *p < 0.05; ***p < 0.001. *n* = (3 eyes, 9 spots)

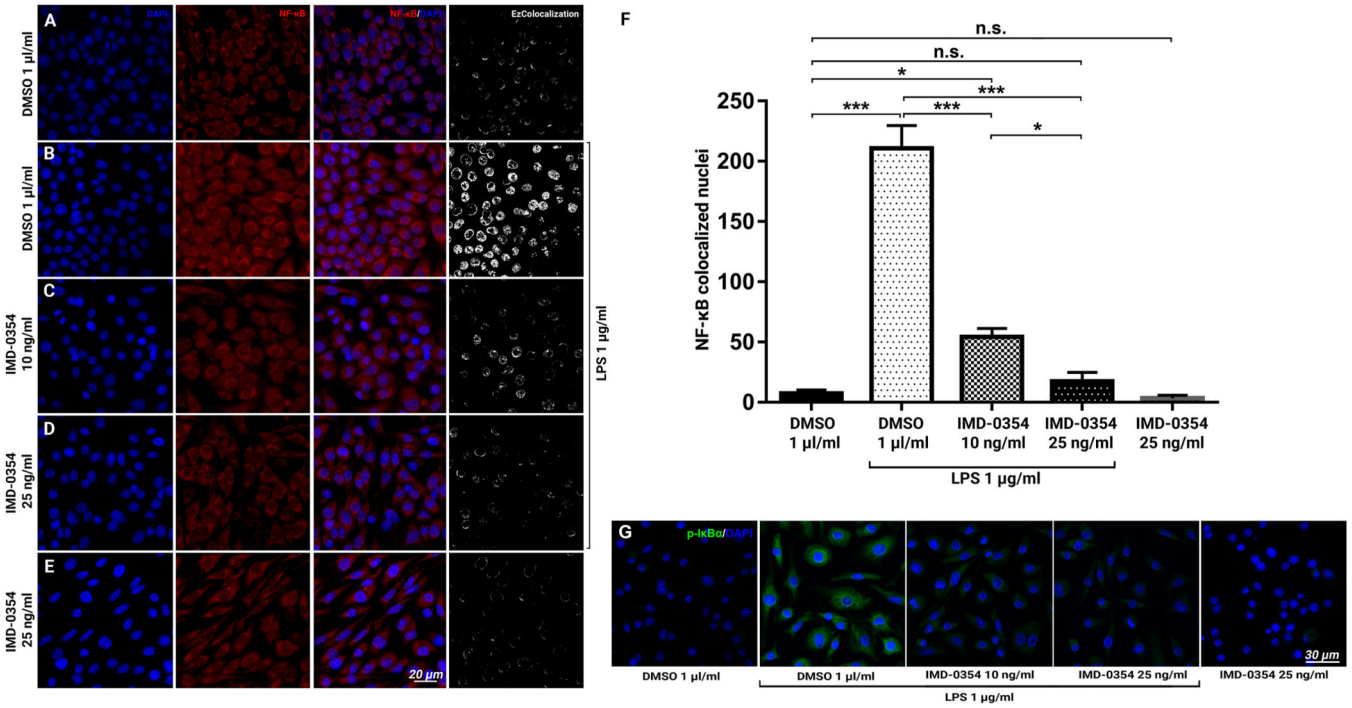

Figure 5:

Effect of IMD-0354 treatment on NF-κB p65 nuclear translocation in LPS-stimulated BV-2 cells.

Inhibitory effect of IMD-0354 (10 ng/ml) on NF-κB (red) nuclear translocation in BV-2 cell cultures. DMSO (1 µl/ml)-treated control, cell nuclei counterstained with DAPI (**A**), LPS 1 µg/ml-stimulated BV-2 cells (**B**), 10 ng/ml IMD-0354 (**C**) and 25 ng/ml IMD-0354 (**D**) with 1 µg/ml LPS stiumulation, demonstrate dose-dependent reduction in nuclear localization of NF-κB. (**E**) IMD-0354 treatment 25 ng/ml without LPS stimulation. (**F**) Quantitative analysis of NF-κB nuclear translocation cells. Statistical significance was determined using one-way ANOVA with Tukey multiple comparisons. *$p < 0.05$; **$p < 0.01$; ***$p < 0.001$. $n = 10$ (**F**) p-IκBα. Immunofluorescent staining in BV-2 cells treated with DMSO (1 µl/ml), LPS 1 µg/ml-stimulated, 10 ng/ml, 25 ng/ml IMD-0354 with 1 µg/ml LPS stimulation and IMD-0354 treatment 25 ng/ml without LPS stimulation.

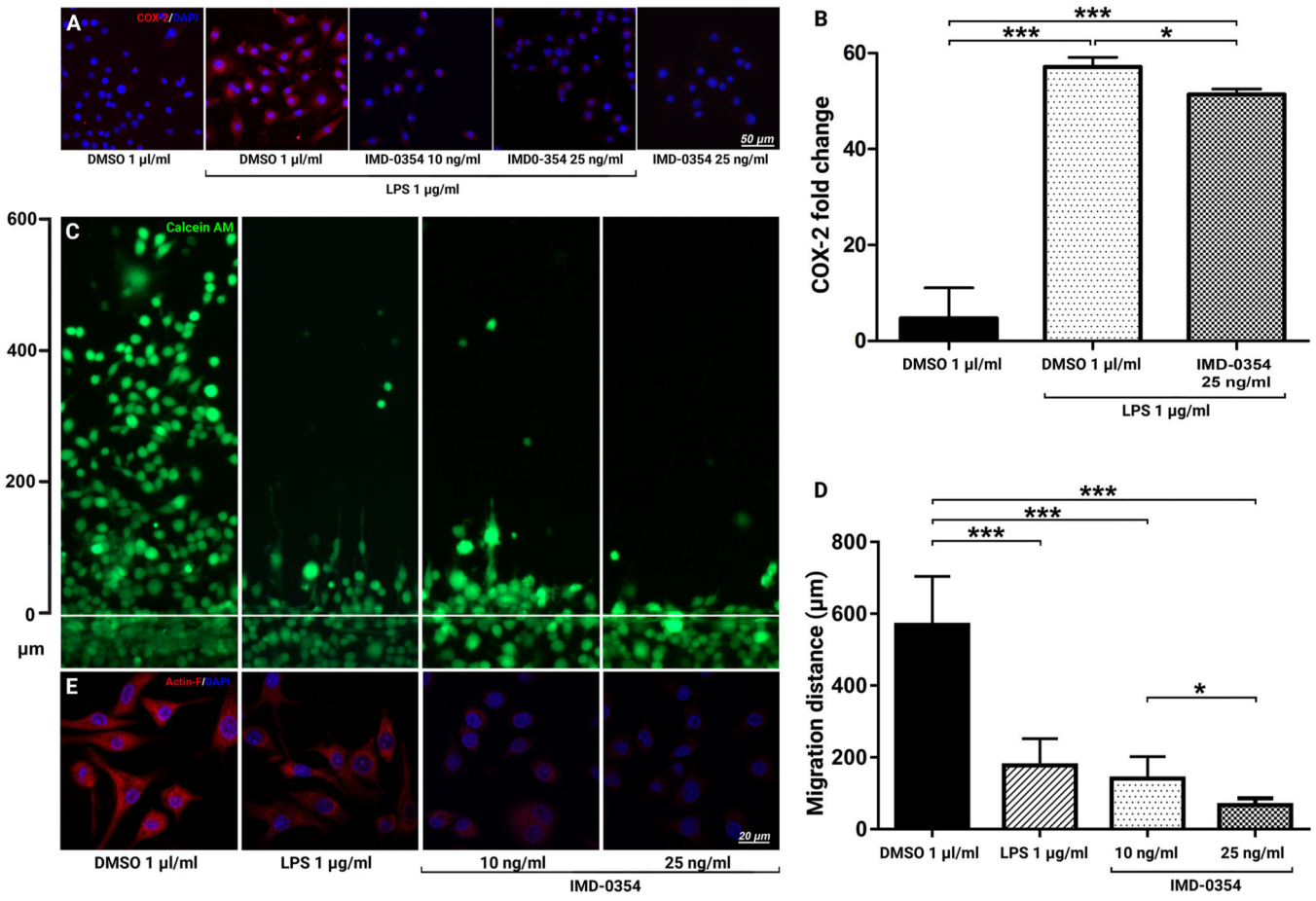

Figure 6:

Effects of IKK2 Inhibition on BV-2 cell activation and motility.

COX-2 expression in LPS-stimulated BV-2 cells treated with IKK2 inhibitor IMD-0354 (**A**). Quantitative qRT-PCR analysis of COX-2 expression ($n = 3$) (**B**). Dose-dependent inhibitory effect of IMD-0354 (10 and 25 ng/ml) on BV-2 cell migration relative to control (1 μl/ml DMSO. Live culture images of BV-2 cells scratch (wound healing) assay cultures treated with DMSO 1 μl/ml, LPS 1 μg/ml, IMD-0354 (10 and 25 ng/ml) 24-hours after induction of the scratch and treatment. BV-2 cells were visualized with Calcein-AM (green) (**C**). Quantification of BV-2 cells migration distance ($n = 8$) (**D**). BV-2 cells F-actin expression and cytoskeletal arrangement in control, LPS 1 μg/ml, IMD-0354 (10 and 25 ng/ml) (**E**). IKK2 Inhibition decreased expression and organization of F-actin filaments in a dose-dependent manner resulting in rounded cell morphology. Statistical significance was determined using one-way ANOVA with Tukey multiple comparisons. *$p < 0.05$; **$p < 0.01$; ***$p < 0.001$.

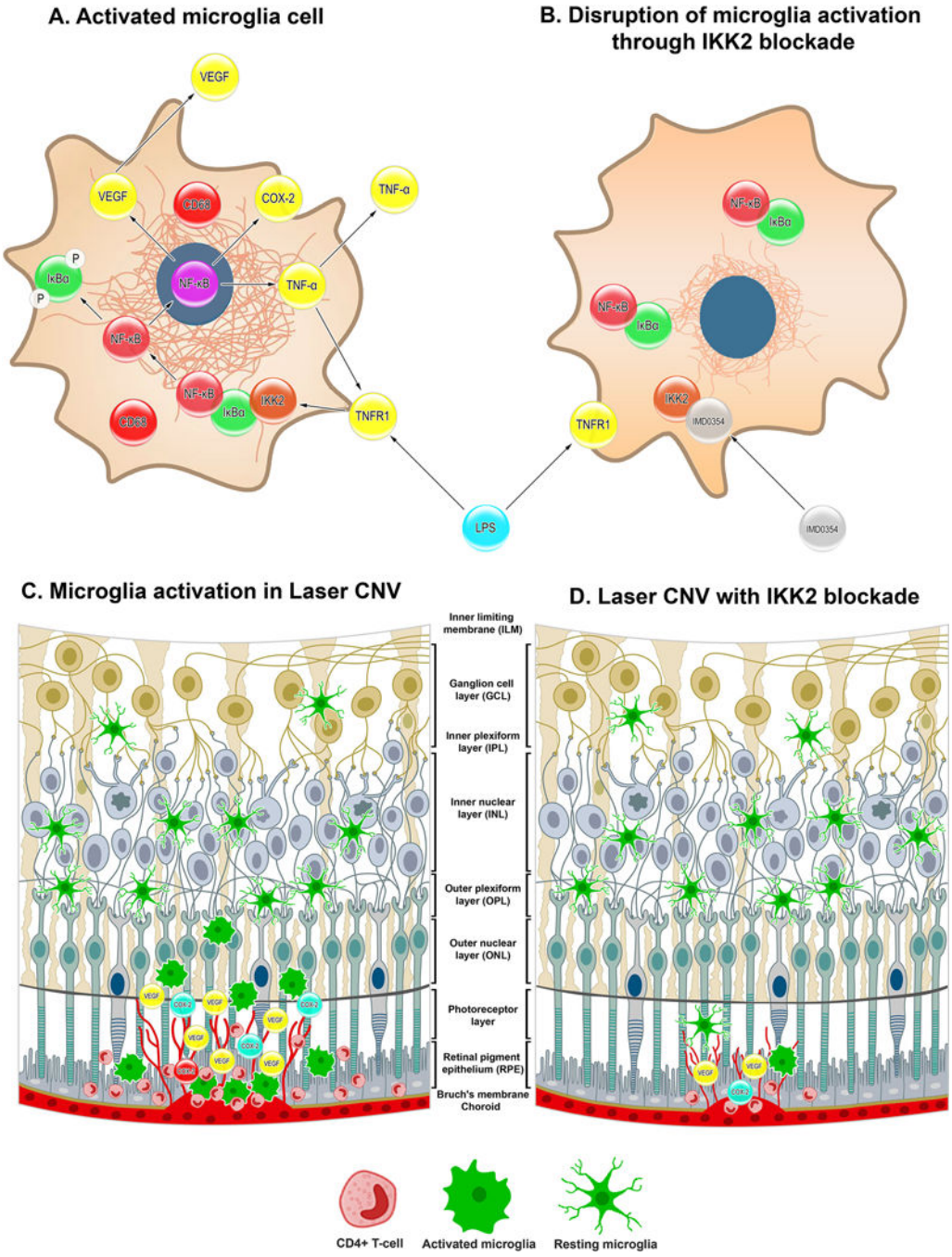

Figure 7:

Graphical summary of the finding.

Cellular level events microglia during proinflammatory insult in control (**A)** and with IKK2 inhibition by IMD-0354 (**B**). Microglia activation and migration towards laser CNV site in control (**C**) and IMD-0354 treated eyes (**D**).

Table 1:

List of primary antibodies used in the study

Target protein	Produced by	Catalog number	Host	IHC dilution	WB dilution
IBA-1	Wako, Fujifilm	019–19741	Rabbit	1:100	-
NFκB p65	Thermo Fisher Scientific	33–9900	Mouse	1:100	-
NFκB p65	Santa Cruz Biotechnology	sc-372	Rabbit	1:100	-
phospho-IκBα	Santa Cruz Biotechnology	sc-8404	Rabbit	1:100	1:500
COX-2	Thermo Fisher Scientific	MA5-14568	Rabbit	1:100	-
VEGFA	Santa Cruz Biotechnology	sc-152	Rabbit	1:50	1:500
CD68	Abcam	Ab201340	Mouse	1:100	-
β-actin	Thermo Fisher Scientific	MA5-15739	Mouse	-	1:2000